

---

# SAFE AND EFFICIENT SOCIAL NAVIGATION THROUGH EXPLAINABLE SAFETY REGIONS BASED ON TOPOLOGICAL FEATURES

---

✉ **Victor Toscano-Duran**,\* ✉ **Rocio Gonzalez-Diaz**

Department of Applied Mathematics I, University of Seville  
Seville, Spain  
{vtoscano, rogodj}us.es

✉ **Sara Narteni**, ✉ **Alberto Carlevaro**, ✉ **Maurizio Mongelli**

CNR-IEIIT  
Genoa, Italy  
{sara.narteni, maurizio.mongelli, albertocarlevaro}@cnr.it

✉ **Jerome Guzzi**

SUPSI, IDSIA  
Lugano, Switzerland  
jerome.guzzi@supsi.ch

## ABSTRACT

The recent adoption of artificial intelligence (AI) in robotics has driven the development of algorithms that enable autonomous systems to adapt to complex social environments. In particular, safe and efficient social navigation is a key challenge, requiring AI not only to avoid collisions and deadlocks but also to interact intuitively and predictably with its surroundings. To date, methods based on probabilistic models and the generation of conformal safety regions have shown promising results in defining safety regions with a controlled margin of error, primarily relying on classification approaches and explicit rules to describe collision-free navigation conditions.

This work extends the existing perspective by investigating how topological features can contribute to the creation of explainable safety regions in social navigation scenarios, enabling the classification and characterization of different simulation behaviors. Rather than relying on behaviors parameters to generate safety regions, we leverage topological features through topological data analysis. We first utilize global rule-based classification to provide interpretable characterizations of different simulation behaviors, distinguishing between safe (free of collisions) and unsafe scenarios based on topological properties. Next, we define safety regions,  $S_\epsilon$ , representing zones in the topological feature space where collisions are avoided with a maximum classification error of  $\epsilon$ . These regions are constructed using adjustable SVM classifiers and order statistics, ensuring a robust and scalable decision boundary. To enhance interpretability, we extract local rules from these safety regions, ensuring that the decision-making process remains transparent and comprehensible.

Initially, we generate safety regions that separate simulations with and without collisions, achieving higher accuracy than methods that do not incorporate topological features. This approach also provides a deeper and more intuitive understanding of robot interactions within a navigable space. We then extend our methodology to design safety regions that ensure efficient simulations (i.e., free of deadlocks). Finally, we integrate both aspects to obtain comprehensive safety regions that guarantee both collision-free and deadlock-free simulations, defining an overall compliant simulation space.

**Keywords** Safe navigation · Explainable artificial intelligence · Safety regions · Topological data analysis · Interpretability

---

\*Corresponding author.

## 1 Introduction

Nowadays, machine learning (ML) and deep learning (DL) play a fundamental role in a wide range of fields [1], with robotics standing out as a domain where autonomous decision-making finds fertile ground. Artificial intelligence (AI) supports a wide range of robotics applications [2], from object detection and recognition to healthcare, manufacturing, and agriculture. One of the most impactful applications of AI in robotics is assistive robotics, where social robots are designed to support everyday tasks, ensuring safe indoor and outdoor navigation while interacting effectively with humans and their surroundings.

However, as autonomous systems become more prevalent in social spaces, ensuring their safety and reliability remains a critical challenge [3]. AI models must operate as intended without harming users or the surrounding environment. To address this, many researchers in safe and explainable AI (XAI) [4] have focused on simulation and validation techniques to assess model reliability.

In particular, topological data analysis (TDA) has emerged as a promising tool in this context, offering new ways to characterize interactions and structures within the navigation space [5, 6]. Within TDA, persistent entropy [7] stands out for its ability to efficiently track the evolution of topological features over time, and can be a robust measure for defining safe and efficient navigation regions and analyzing robot-agent interactions.

In this work, we address a simulated social navigation scenario inspired by human movement, where robots navigate between pairs of opposing targets, facing potential risks of collision and deadlock. These challenges compromise both the safety and efficiency of mobile navigation. To tackle this issue, we leverage topological features, specifically from persistent entropy, as input data to classify and characterize different simulation behaviors.

In a fleet of robots, topological features provide a quantifiable representation of the spatial structures that emerge during navigation, capturing patterns such as clustering, dispersion, and movement coordination. This allows us to systematically distinguish between safe (collision-free) and unsafe scenarios. By utilizing global rule-based classification, adjustable SVM classifiers, and order statistics, we construct safety regions that not only prevent collisions but also enhance navigation efficiency by avoiding deadlocks. Finally, we integrate these aspects to define a compliant navigation space, ensuring both collision-free and deadlock-free simulations. This approach supports the development of robust and explainable AI models, where topological insights can enhance transparency and performance in defining safe (without collisions), efficient (without deadlocks), and compliant (free of collisions and deadlocks) navigation strategies.

The remainder of the article is organized as follows: first, in Section 2, we present the state of the art and existing literature in the field. Section 3 introduces the preliminary concepts relevant to this study, including topology, confidence regions, and rule-based models, as well as the simulation-based robotic navigation environment. Section 4 details the proposed methodology for constructing safety regions regarding the topological feature space. Section 5 provides a comprehensive explanation of the experiments conducted, along with the results obtained. Finally, conclusions and future work are discussed in Section 6.

## 2 Related work

The integration of machine learning (ML) and deep learning (DL) into robotics [8] has accelerated the capabilities of autonomous systems across various fields. Particularly within assistive and social robotics, the objective has evolved from simple navigation to enabling safe and interpretable decision-making around people. Early works on ML for robotics primarily focused on object detection and recognition [9, 10], yet more recent efforts leverage DL algorithms to enhance contextual understanding and adaptive navigation. These advancements have led to behavioral AI models capable of dynamically adjusting to complex, changing environments, such as crowded indoor spaces while ensuring user safety.

The concept of explainable AI (XAI) [11, 12, 4] has emerged as a necessary framework to improve AI transparency and trustworthiness [13], particularly in safety-critical applications like social robotics. In this context, several studies propose the use of simulation and validation techniques to evaluate ML models before deployment in real-world scenarios, emphasizing safety and reliability in decision-making [14, 15]. Additionally, explainability and interpretability enhance user trust, as evidenced in approaches like rule-based reinforcement learning and fuzzy logic systems for robotic risk mitigation, which incorporate predefined standards and probabilistic safety regions to guide exploration while minimizing risk and redundant actions [16, 17].

To address this, topological data analysis (TDA) provides novel tools for examining complex data structures, making it possible to extract and interpret information about the underlying structure of navigational spaces. TDA techniques, such as persistent homology [18, 19, 20], have been applied to analyze spatial connectivity and the evolving structures

within navigation environments [21, 22, 23], offering a quantifiable approach to characterize spatial and behavioral patterns over time. Persistent entropy [24], a summarization of persistent homology, quantifies the complexity of topological features over time, and is especially useful in scenarios where robots may need to navigate shared spaces while avoiding collisions and deadlocks to ensure safe and efficient navigations.

Moreover, persistent entropy has demonstrated its effectiveness in a variety of other applications such as characterizing idiotypic immune networks [25], analyzing similarities in piecewise linear functions and time series [7], and separating topological features from noise in Vietoris-Rips complexes [26]. These successful applications underscore its versatility and potential to provide robust insights across diverse domains.

The integration of TDA into the analysis of robotic systems marks a step forward in developing explainable models for safe navigation. This approach allows us to detect, quantify, and analyze safety regions, focusing on spatial structures formed by robots in motion [27]. By combining TDA with simulated environments, we contribute to the growing field of XAI for robotics by facilitating a more interpretable approach to parameter tuning within navigation models. This directly contributes to improving safety and reliability in socially aware robotic systems, offering the potential for broader applications in real-world, and human-centric environments [28].

### 3 Background

This section presents all preliminary concepts that are used throughout the paper. It begins by introducing topological foundations (Section 3.1), including an exploration of topological spaces and simplicial complexes as fundamental structures. Persistent homology and persistent entropy are also discussed, as they provide insights into the geometry and connectivity of data. Subsequently, the focus shifts to confidence regions (Section 3.2), defining safety regions based on probabilistic scaling and conformal prediction methods. These techniques ensure robust predictions with statistical guarantees. It continues explaining rule-based models (Section 3.3), emphasizing interpretability through global and local rule-extraction techniques, such as Anchors. However, these techniques often struggle to capture the underlying geometric and topological structure of data, limiting their ability to generalize across complex decision boundaries. To address this, the proposed methodology in Section 4 leverages topological features as inputs to enhance model interpretability and robustness. This subsection also highlights evaluation metrics like coverage and error for assessing rule-based classifiers’ performance. To apply these concepts, as well as the methodology proposed in this paper, which is explained in Section 4, to the field of robotic navigation, a social robotics navigation simulator is employed, called Navground (described in Section 3.4). This simulator allows for testing navigation algorithms within multi-agent systems and evaluating their performance in diverse scenarios.

#### 3.1 Topology Background

**Topology and Topological Space.** A topological space is a powerful mathematical concept for describing the connectivity of a space. Informally, a topological space is a set of points, each of them equipped with the notion of neighbourhood.

One way to represent a topological space is by decomposing it into simple pieces such that their common intersections are lower-dimensional pieces of the same kind. In this paper, we use simplicial complexes as the data structure to represent topological spaces.

**Simplicial Complex.** An *abstract simplicial complex*  $\mathcal{K}$  is given by:

- A set  $V$  of 0-simplices (also called vertices);
- For each  $k \geq 1$ , a set of  $k$ -simplices  $\sigma = \{v_0, v_1, \dots, v_k\}$ , where  $v_i \in V$ ;
- Each  $k$ -simplex has  $k + 1$  faces obtained by removing one of the vertices;
- If  $\sigma$  belongs to  $\mathcal{K}$ , then all the faces of  $\sigma$  must belong to  $\mathcal{K}$ .

A *simplicial complex*  $K$  is a geometric realization of an abstract simplicial complex  $\mathcal{K}$  [29]. It is constructed as a nested family of simplices, where each simplex is a generalization of geometric shapes of various dimensions. Specifically, a 0-simplex corresponds to a point in a given Euclidean space  $\mathbb{R}^n$ , a 1-simplex represents an edge, a 2-simplex is a filled triangle, a 3-simplex is a filled tetrahedron, and so on. This hierarchical structure allows the simplicial complex to model higher-dimensional relationships between points in a mathematically rigorous way.

Homology groups are algebraic structures that describe features of a topological space  $\mathcal{C}$ . The  $k$ -th Betti number represents the rank of the  $k$ -dimensional homology group. Informally, for a fixed  $k$ , the  $k$ -th Betti number  $\beta_k$  counts the number of  $k$ -dimensional holes characterizing  $\mathcal{C}$ :  $\beta_0$  is the number of connected components,  $\beta_1$  counts the number of

holes in  $2D$  or tunnels in  $3D$ <sup>2</sup>,  $\beta_2$  can be thought of as the number of voids in geometric solids. In this work, we use simplicial homology, which consists of computing homology groups of simplicial complexes.

See [18, 30] for an introduction to algebraic topology.

**Persistent Homology.** Topological data analysis, particularly persistent homology, has emerged as a valuable approach for studying the geometry and connectivity of datasets that evolve over time or space [27]. The primary objective of employing topological data analysis tools, like persistent homology and persistent entropy, in the context of fleet behavior modeling is to achieve a more nuanced understanding of system dynamics.

Persistent homology is a method for computing  $k$ -dimensional holes at different spatial resolutions. In this section, we briefly explain how this method works. For a more formal description, we refer the reader to [20].

In order to compute persistent homology, we need a nested sequence of increasing subcomplexes. More formally, a *filtered simplicial complex* or, for short, a *filtration* is a collection of subcomplexes  $\{K(t) \mid t \in \mathbb{R}\}$  of a simplicial complex  $K$  such that  $K(t) \subseteq K(s)$  for  $t < s$  and there exists  $t_{\max} \in \mathbb{R}$  such that  $K(t_{\max}) = K$ . The *filtration time* (or filter value) of a simplex  $\sigma \in K$  is the smallest  $t$  such that  $\sigma \in K(t)$ . An example of a filtered simplicial complex is depicted in Fig. 1.

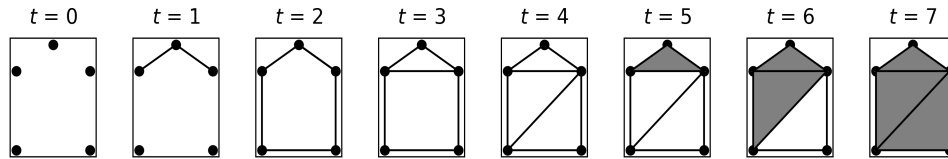


Figure 1: A filtration for  $t = 0, 1, 2, 3, 4, 5, 6, 7$  (from left to right).

Persistent homology describes how the homology of  $K$  changes along a filtration  $\{K(t) \mid t \in \mathbb{R}\}$ . A  $k$ -dimensional *Betti interval*, with endpoints  $[t_{\text{start}}, t_{\text{end}})$ , corresponds to a  $k$ -dimensional hole that appears at filtration time  $t_{\text{start}}$  and remains until time  $t_{\text{end}}$ .

To visualize the persistence of topological features, persistence diagrams are commonly used. **Persistence diagrams** are visual representations used in the study of persistent homology to illustrate the birth and death of topological features (such as connected components, loops, and voids) as the scale of observation changes. It consists in a set of points  $(b_i, d_i) \in \mathbb{R}^2$  (with  $b_i \leq d_i$ ). Each point represents the birth ( $b_i$ ) and death ( $d_i$ ) of a topological feature in a filtered space. Instead of points, we sometimes draw intervals representing the birth and death times of homology classes. This method, also known as **persistence barcodes** [31], provides an alternative visualization of the same information contained in persistence diagrams, plotting this data in bars. Each bar in the barcode corresponds to a topological feature and is represented by an interval  $[b_i, d_i)$ . An illustrative example of a persistence diagram and a persistence barcode is in Fig. 2.

**Persistent entropy.** In order to measure how much the construction of a filtered simplicial complex is ordered, an entropy measure, called persistent entropy, was defined in [7]. A precursor of this definition was given in [24] to measure how different bars of a persistence barcode are in length. In other words, persistent entropy is a measure of the complexity of a topological space based on its persistence diagram.

Given a filtered simplicial complex  $\{K(t) : t \in \mathbb{R}\}$ , and the corresponding persistence diagram  $D = \{(b_i, d_i) : i \in I\}$ , where  $b_i \leq d_i$  for all  $i \in I$ , and  $I$  is the index set that identifies the pairs  $(b_i, d_i)$  in  $D$ . As commented previously, each pair  $(b_i, d_i)$  corresponds to a topological feature that “appears” at time  $b_i$  (birth) and “disappears” at time  $d_i$  (death) as the filtration progresses. The *persistent entropy*  $H$  of a filtered simplicial complex  $K$  is calculated as follows:

$$H = - \sum_{i \in I} p_i \ln p_i \quad (1)$$

where  $p_i = \frac{\ell_i}{L}$ ,  $\ell_i = d_i - b_i$ , and  $L = \sum_{i \in I} \ell_i$ .

It is important to note that this formulation considers only the duration  $\ell_i$  of each topological feature (bar), rather than its starting time  $b_i$ . This is because persistent entropy aims to capture the distribution of topological feature lifetimes rather than their birth times. Ignoring starting times ensures that the measure remains invariant under time shifts in the filtration, making it more robust for comparing different persistence barcodes. In particular, we focus on dimension

<sup>2</sup> $dD$  refers to the  $d$ -dimensional space  $\mathbb{R}^d$

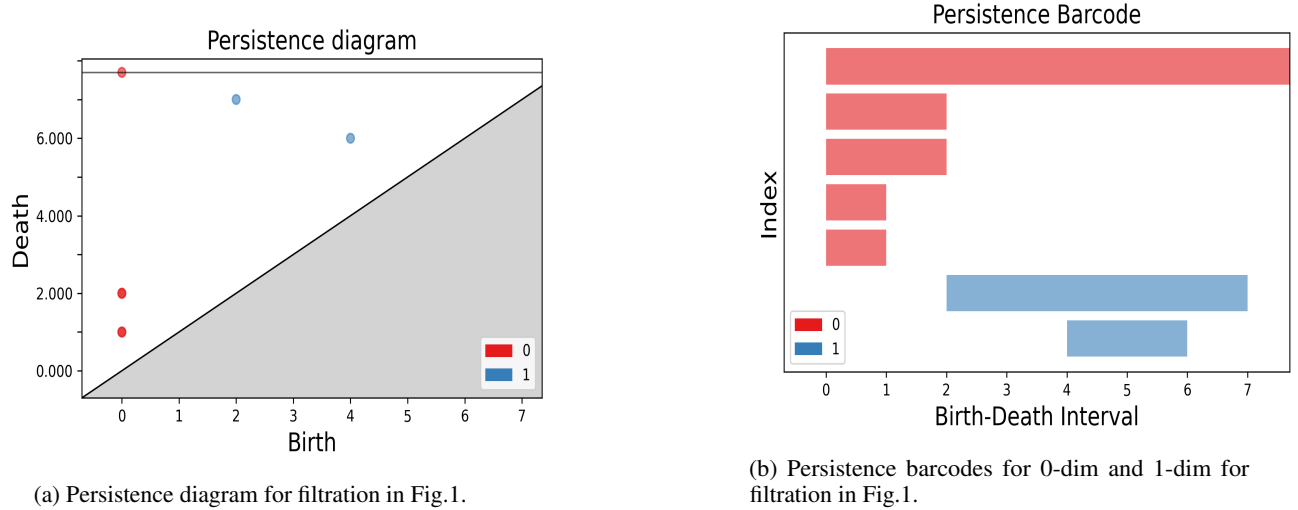


Figure 2: Persistence diagram and persistence barcode example.

0, which is characterized by the fact that all features in this dimension are born at the same instant but have different durations, meaning some persist longer than others.

The maximum persistent entropy corresponds to the situation in which all the intervals in the barcode are of equal length. In that case,  $H = \ln n$ , where  $n$  is the number of elements of  $I$ . In contrast, the value of the persistent entropy decreases as more intervals of different lengths are present. A potential point of confusion arises because persistent entropy does not measure the entropy of the distribution of bar lengths directly. Instead, it measures the entropy of the probability distribution induced by the relative contributions of each bar to the total barcode length. If all bars had the same length, their contributions would be equal, maximizing entropy. Conversely, when some bars dominate the total length, entropy decreases. Thus, persistent entropy should be interpreted as the entropy of the distribution of bar indices weighted by their respective lifetimes, rather than the entropy of the length distribution itself.

For example, for the persistence barcode of dimension 0 in Fig. 2b, we have 5 bars with the following lengths  $l_i$ : 1, 1, 2, 2, 8, obtaining a total length  $L$  of 14. Thus, the probabilities ( $p_i$ ) in this case are:  $\frac{1}{14}$ ,  $\frac{1}{14}$ ,  $\frac{2}{14}$ ,  $\frac{2}{14}$ , and  $\frac{8}{14}$ , resulting in a persistent entropy of 1.25. A different distribution of the same points producing lower or higher persistent entropy indicates that the points are more concentrated or dispersed, respectively.

### 3.2 Background on Confidence Regions

Here, the concept of *probabilistic safety region* is introduced, which we define as the subset of the input space where probabilistic guarantees for the prediction of a target (safe) class are provided. This approach begins with a discussion of adjustable classifiers, a specialized class of classifiers whose boundaries can be adjusted by a scalar parameter. This adjustability facilitates the construction of safety regions that offer reliability in classification by adjusting boundaries to meet specific performance metrics, such as minimizing false positives.

Following this, we integrate adjustable classifiers with two statistical approaches: probabilistic scaling and conformal prediction. These methods construct the desired safety regions with probabilistic assurances, which can be applied to machine learning classifiers without specific assumptions on the underlying data distribution.

**Adjustable Classifiers.** Consider an input space  $X \subseteq \mathbb{R}^d$  and an output space  $Y = \{-1, +1\}$ , where a binary adjustable classifier is defined as:

$$\phi_{\theta}(x, \rho) = \begin{cases} +1, & \text{if } f_{\theta}(x, \rho) < 0, \\ -1, & \text{otherwise.} \end{cases} \quad (2)$$

Here,  $f_{\theta} : X \times \mathbb{R} \rightarrow \mathbb{R}$  is the classifier predictor. The function  $f_{\theta}(x, \rho)$  is dependent on tunable hyperparameters  $\theta$  and an adjustable scalar  $\rho$ , which shifts the classification boundary, allowing for control over the classifier’s performance, such as adjusting the false positive rate. Any classifier,  $\hat{f}(x)$ , can be made adjustable by adding  $\rho$  as an offset:

$f_\theta(x, \rho) = \hat{f}_\theta(x) + \rho$ . A Support Vector Machine (SVM) classifier can thus be adapted as  $f_\theta(x, \rho) = w^T \varphi(x) - b + \rho$ , where  $w$  is the vector of the learned weights,  $\varphi$  is a feature map and  $b$  is the offset.

For each point  $x$ , we define  $\bar{\rho}(x)$  as the  $\rho$  value where  $x$  is on the decision boundary, i.e.,  $f_\theta(x, \bar{\rho}(x)) = 0$ . This framework enables defining the  $\rho$ -safe set:

$$S(\rho) = \{x \in X : f_\theta(x, \rho) < 0\}, \quad (3)$$

which is the region classified as safe (+1). However, this set alone does not ensure a probabilistic guarantee, only that the classifier predicts +1 within this region. To obtain a probabilistic safety region  $S_\epsilon$  that satisfies  $P(y = -1 | x \in S_\epsilon) \leq \epsilon$  with confidence  $1 - \delta$ , techniques from the field of order statistics can be used, such as probabilistic scaling and conformal prediction.

**Probabilistic Scaling.** Probabilistic scaling (SP) constructs safety regions based on the order statistics of the calibration dataset  $Z_c = \{(x_i, y_i)\}_{i=1}^{n_c} \subset X \times Y$ . We define the generalized maximum  $\max_{(r)}(\Gamma)$  for a set  $\Gamma = \{\gamma_i\}_{i=1}^n \in \mathbb{R}^n$  as the  $r$ -th largest value, ensuring no more than  $r - 1$  elements of  $\Gamma$  exceed  $\max_{(r)}(\Gamma)$ . Assuming a continuous and monotonically increasing  $f_\theta(x, \rho)$  on  $\rho$ , probabilistic scaling yields a  $\rho_\epsilon$  such that:

$$S_\epsilon = S(\rho_\epsilon), \quad (4)$$

where  $\rho_\epsilon$  is computed to satisfy  $P(y = -1 | x \in S_\epsilon) \leq \epsilon$  with probability  $1 - \delta$ . Details and assumptions for this method are provided in [16].

**Conformal Prediction.** Conformal prediction (CP), as developed in [32], provides a post-hoc assessment of classification conformity. Using a score function  $s : X \times Y \rightarrow \mathbb{R}$ , such as  $s(x, \hat{y}) = -\hat{y}\bar{\rho}(x)$ , that encodes the agreement between a sample  $x$  and a candidate label  $\hat{y}$ , CP defines a prediction region  $C_\epsilon(x)$ :

$$C_\epsilon(x) = \{\hat{y} \in \{-1, +1\} : s(x, \hat{y}) \leq s_\epsilon\}, \quad (5)$$

ensuring marginal coverage  $P(\hat{y} \in C_\epsilon(x)) \geq 1 - \epsilon$ . From this, the conformal safety region  $\Sigma_\epsilon$  for input  $x$  with class +1 can be derived, i.e.:

$$\Sigma_\epsilon = \{x \in X : s(x, +1) \leq s_\epsilon, s(x, -1) > s_\epsilon\}, \quad (6)$$

which is such that  $S_\epsilon \subseteq \Sigma_\epsilon$ . In [33] is shown that if  $s_\epsilon \leq 0$  then  $S_\epsilon = \Sigma_\epsilon$ , achieving the desired confidence region. Details about conformal safety region (CSR) are provided in [33].

In the following, we will denote the safety region  $S_\epsilon$  using the two methods as  $S_\epsilon^{PS}$  for the probabilistic scaling method and  $S_\epsilon^{CP}$  for the conformal prediction method.

### 3.3 Rule-Based Models Background

Rule-based classifiers are machine learning models that provide outputs as sets of decision rules (rulesets), offering interpretability [34, 35]. Different techniques for rule-based classification are typically grouped by their scope, based on whether they aim at providing explanations globally valid on the whole dataset, or locally on specific instances [4].

**Global Rule Classifiers.** In this kind of approach, the model learns a set of rules that represent the entire logic of the dataset, making it suitable for application to any data sample. The rules are “native” as they arise directly from the learning process without needing any intermediary steps.

Formally, a rule-based classifier trained on a dataset  $T = \{(x_j, y_j)\}_{j=1}^N \in X \times Y$ , where  $x_j \in \mathbb{R}^d$  and  $y_j \in \{-1, +1\}$ , generates a ruleset  $\mathcal{R} = \{r_k\}_{k=1}^M$ . Each rule  $r_k$  has a premise, or antecedent, expressed as a conjunction of conditions:

$$premise(r_k) = \bigwedge_{i=1_k}^{N_k} c_{ik},$$

where each condition  $c_{ik}$  specifies an interval on the input features, either bounded, left-bounded, or right-bounded. The rule’s consequence specifies the target class  $\hat{y}_k \in \{-1, +1\}$  associated with the premise.

**Local Rule Extraction via Anchors.** Anchors is a model-agnostic local rule extraction technique that generates high-precision rules for explaining individual predictions of any black-box classifier. While locally faithful, these rules also hold in a neighborhood (or perturbation space) of the instance being explained. An anchor  $A$  for an instance  $x$  is a set of predicates that satisfies the precision threshold  $\lambda_{prec}$  with a confidence level  $1 - \delta$ :

$$\Pr\{\text{Prec}(A) \geq \lambda_{prec}\} \geq 1 - \delta,$$

where  $\delta \in [0, 1]$  and  $\lambda_{\text{prec}} \in [0, 1]$  sets the precision requirement for the anchor. Precision  $\text{Prec}(A)$  is defined as:

$$\text{Prec}(A) = \mathbb{E}_{D_x(z|A)} [\mathbb{1}_{f(x)=f(z)}],$$

where  $f$  is the black-box model, and  $D_x(z|A)$  is the distribution of perturbations  $z$  around  $x$  when the anchor applies. Optimal anchors are searched using reinforcement learning, and the process is formulated as a combinatorial optimization problem:

$$\max_A C(A) \quad \text{s.t.} \quad \Pr\{\text{Prec}(A) \geq \lambda_{\text{prec}}\} \geq 1 - \delta,$$

where  $C(A)$  represents the coverage for candidate anchor  $A$ .

**Rule Evaluation.** For rule-based classifiers, the performance of each rule  $r_k$  can be measured with two key metrics—coverage  $C(r_k)$  and error  $E(r_k)$ —that allow us to evaluate the rule’s ability to generalize to unseen data. Before defining the metrics, it is worth underlining that a ‘positive’ instance, in this context, refers to any instance that satisfies the considered rule, regardless of the output class. Similarly, the term ‘negative’ is used to denote the case when points do not satisfy the rule.

**Coverage**  $C(r_k)$ : this measures the proportion of correctly classified positive samples by rule  $r_k$ :

$$C(r_k) = \frac{\text{TP}(r_k)}{\text{TP}(r_k) + \text{FN}(r_k)},$$

where  $\text{TP}(r_k)$  is the count of true positives and  $\text{FN}(r_k)$  is the count of false negatives associated with the rule.

**Error**  $E(r_k)$ : it represents the proportion of false positives in the total predictions, helping to gauge rule precision:

$$E(r_k) = \frac{\text{FP}(r_k)}{\text{TN}(r_k) + \text{FP}(r_k)},$$

where  $\text{FP}(r_k)$  and  $\text{TN}(r_k)$  represent false positives and true negatives, respectively.

Combined, coverage and error contribute to the **relevance**  $R(r_k)$  of each rule, which indicates its generalizability:

$$R(r_k) = C(r_k) \cdot (1 - E(r_k)).$$

### 3.4 Simulation of Social Robotics Navigation

Hinted by its name, Navground<sup>3</sup> is a playground to experiment with navigation algorithms. The Navground social navigation simulator allows for experimentation with various navigation algorithms. At its core, the simulator operates with multi-agent (robots) systems that carry out specific navigation tasks, ensuring they avoid collisions with both static obstacles and other robots, and deadlocks. Each robot is represented as a circular disc, with its state defined by a  $2D$  pose ( $x$  and  $y$ ), its orientation angle and its *twist*; the velocity of the robot in the  $x$ -axis direction, its velocity in the  $y$ -axis direction and its rotational speed, in radians per second, around its central axis, which represents how fast the robot turns. Robots navigate using one of several reactive navigation behaviors, which consider the current state of the environment to generate control commands that guide them toward their targets while avoiding collisions.

In this article, robots are modelled after the Thymio robot, a small robot with a size of 8 cm and two-wheel differential-drive kinematics, which is a very common kinematics<sup>4</sup> shared by many ground robots. Each simulated robot executes a specific behavior. In this article, robots will follow the *human-like* (HL) navigation [36], which is a bio-inspired, computationally light, local navigation algorithm for robotics, adapting a heuristic model for pedestrian motion. It addresses engineering aspects such as trajectory effectiveness and scalability, as well as societal aspects by producing human-friendly, predictable trajectories. In other words, this behavior is inspired by the way the pedestrian moves.

The HL navigation algorithm operates in regular time intervals by following three key steps: first, it selects the best direction toward the target while avoiding potential collisions by considering a safety margin around the robot and the velocity of nearby entities. Second, it determines an appropriate speed that allows the robot to stop within a safe distance if needed. Finally, the velocity is smoothly adjusted over time to ensure natural movement transitions. The safety of the resulting trajectories depends on various parameters (see Tab. 1 for the explanation of some HL parameters), such as the safety margin  $\sigma$ , which helps account for modeling and perception errors.

Additionally, Navground provides different scenarios, where robots can navigate, in order to test and analyze their behavior. In this article, we will use the *crossings* scenario. In this scenario, we define the variable  $s$  as the length

<sup>3</sup><https://github.com/idsia-robotics/navground>

<sup>4</sup>Kinematics is the study of the relationship between a robot’s joint coordinates and its spatial layout, and is a fundamental and classical topic in robotics.

Table 1: Description of HL Parameters

Parameter	Description
$v_{\text{opt}}$	The desired optimal speed
$\tau_{\text{rot}}$	The relaxation time to rotate towards a desired orientation
$\sigma$ (safety margin)	The minimal safety margin (distance) to keep away from obstacles or other robots
$\eta$ (eta)	The time that the behavior keeps away from collisions
$\tau$ (tau)	The relaxation time controlling the smoothness of the motion

of each side of the square area containing the target waypoints and define the operational space for robots. The four target waypoints are located at the following coordinates:  $(-\frac{s}{2}, 0)$ ,  $(\frac{s}{2}, 0)$ ,  $(0, -\frac{s}{2})$ , and  $(0, \frac{s}{2})$ . Half of the robots are tasked to pendle between the two vertically aligned waypoints, and half between the horizontally aligned waypoints (see Fig. 3). The scenario tests how robots cross in the middle, where the 4 opposing flows meet. In the case of the cross scenario, we must be clear that the positions of the robots go on the  $x$ -axis from  $-\frac{s}{2}$  to the value set in  $\frac{s}{2}$  of the scenario, and on the  $y$ -axis similarly.

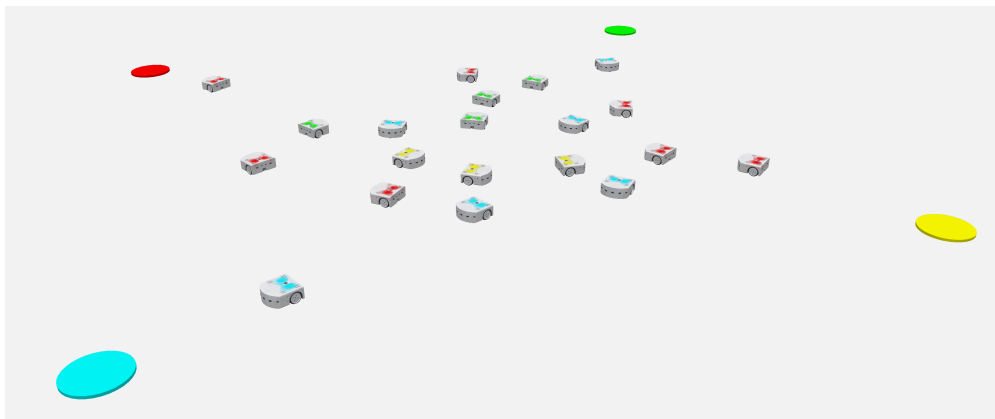


Figure 3: Point cloud representation of robot positions in the “cross” scenario. In this setup, robots navigate between predefined waypoints (colored cylinders) along the  $x$ -axis and  $y$ -axis, creating intersecting flows at the center.

In addition, in the context of social navigation between robots, deadlocks and collisions refer to two different types of issues that can arise during the interaction and navigation of multiple robots in a shared environment. A deadlock in robot navigation occurs when one or more robots become trapped in a situation where they cannot move due to the positions of other robots, waiting for the other to move in order to take up the movement again. A collision occurs when two or more robots collide or when a robot collides with static obstacles in the environment. This can result from uncoordinated movements or errors in navigation planning and control. We will also focus on these two negative events in experiments. Notice that a simulation can be considered safe if there is no collision between robots, efficient if no robot enters a deadlock state at any point during the simulation, and compliant if there are neither collisions nor deadlocks.

#### 4 Topology-Driven Safety Methodology

Once all preliminary concepts have been defined, we can present the core contribution of this paper: a **topology-driven methodology** for defining safety regions in robot simulations. By combining topological tools with entropy-based analysis, we provide a systematic approach to avoid/prevent unsafe events such as robot collisions or deadlocks.

At a high level, our methodology consists of the following steps (see Fig. 4 for an example):

1. **Simulate:** Generate multiple navigation scenarios where a fleet of mobile robots moves between opposing targets, potentially leading to collisions or deadlocks.
2. **Build a dataset:** Extract topological features from each simulation and assign a binary safety label based on observed events (e.g., presence or absence of collisions). This process consists of the following steps:
  - (a) **Extract point clouds:** From each simulation run performed by Navground, we extract the positions of all robots at each time step, resulting in  $n$  point clouds. Then, for each point cloud, we perform steps b–e.



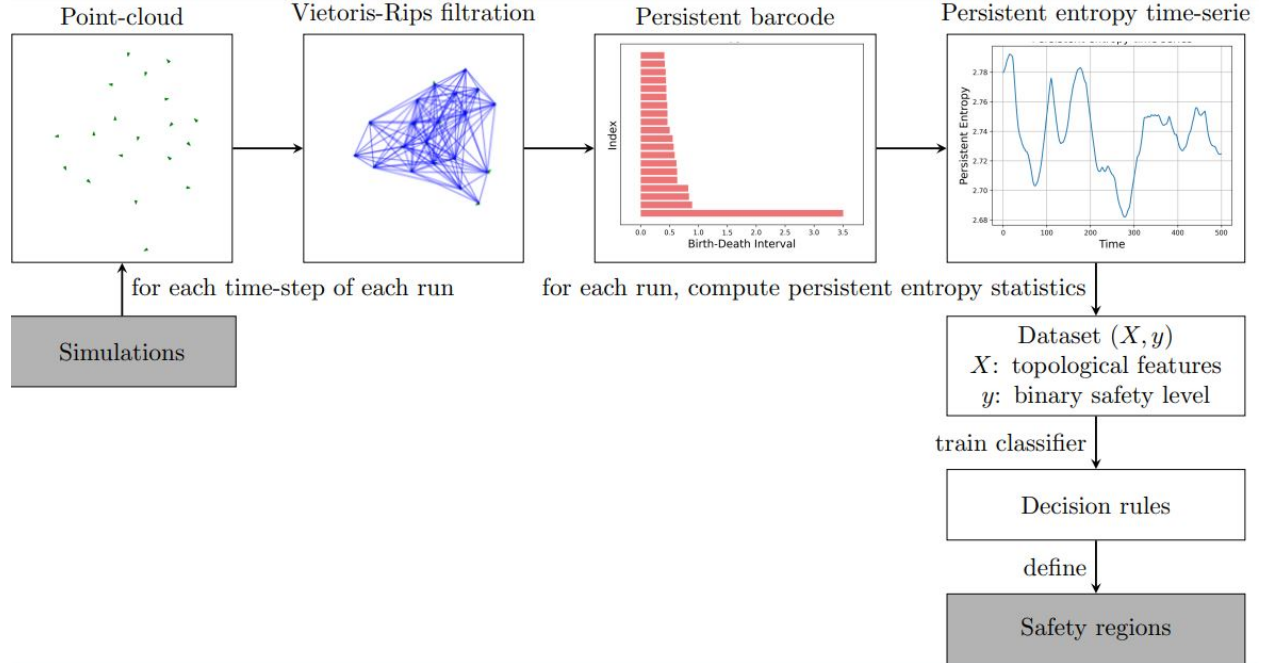


Figure 4: Illustrative example of methodology pipeline.

- (b) **Compute persistent homology:** We compute the persistent homology of the point cloud, using the Vietoris-Rips complex. This yields a **persistence barcode**, focusing only on 0-dimensional features.
- (c) **Analyze birth-death intervals:** From the persistence barcode, we extract the lengths of the intervals that correspond to the 0-dimensional topological features.
- (d) **Normalize interval lengths:** We compute the sum of all interval lengths and normalize each length by this sum, obtaining a probability distribution of interval lengths.
- (e) **Calculate entropy:** We compute the entropy of the probability distribution, using the Shannon entropy formula Eq. (1). See Fig. 5 for an example of a point cloud corresponding to the position of the robots in a specific time step, the corresponding persistence barcode of dimension 0, and the corresponding persistent entropy.
- (f) **Generate time series and statistical parameters.** Once the above process is done for each time step of the simulation, we obtain a persistent-entropy time series for the whole simulation. Finally, we compute four key statistical parameters for this time series: **mean, median, standard deviation and interquartile range (IQR)**. See Fig. 6 for an example of persistent entropy time series over a 500-step simulation.

Once the topological features are extracted, we construct a labeled dataset to train a classifier. The dataset is defined as:

- Input  $x$ : A feature vector extracted from the topological data of the simulation, defined as:  $x = (\text{meanEntropy}, \text{medianEntropy}, \text{stdEntropy}, \text{iqrEntropy})$ . These features are derived from the 6-step methodology explained above.
- Output  $y$ : A binary label indicating whether the simulation is safe(+1) or unsafe(-1). The definition of “safe” depends on the context. Given a set of simulations, we assign each simulation a binary level indicating its safety level, depending on the avoidance event, for example, for safe analysis (collision or not collision):

$$y_i = \begin{cases} +1 & \text{if the number of collisions during the simulation } i \text{ equals 0,} \\ -1 & \text{if the number of collisions during the simulation } i \text{ is greater than 0.} \end{cases}$$

3. **Train a classifier:** Using this dataset, we train a Support Vector Machine (SVM) classifier with adjustable margins to learn the decision function separating safe and unsafe simulations.
4. **Define safety regions:** Once the classifier is trained, we use it to construct probabilistic safety regions, which define zones in the topological feature space where simulations are likely to be safe. These regions

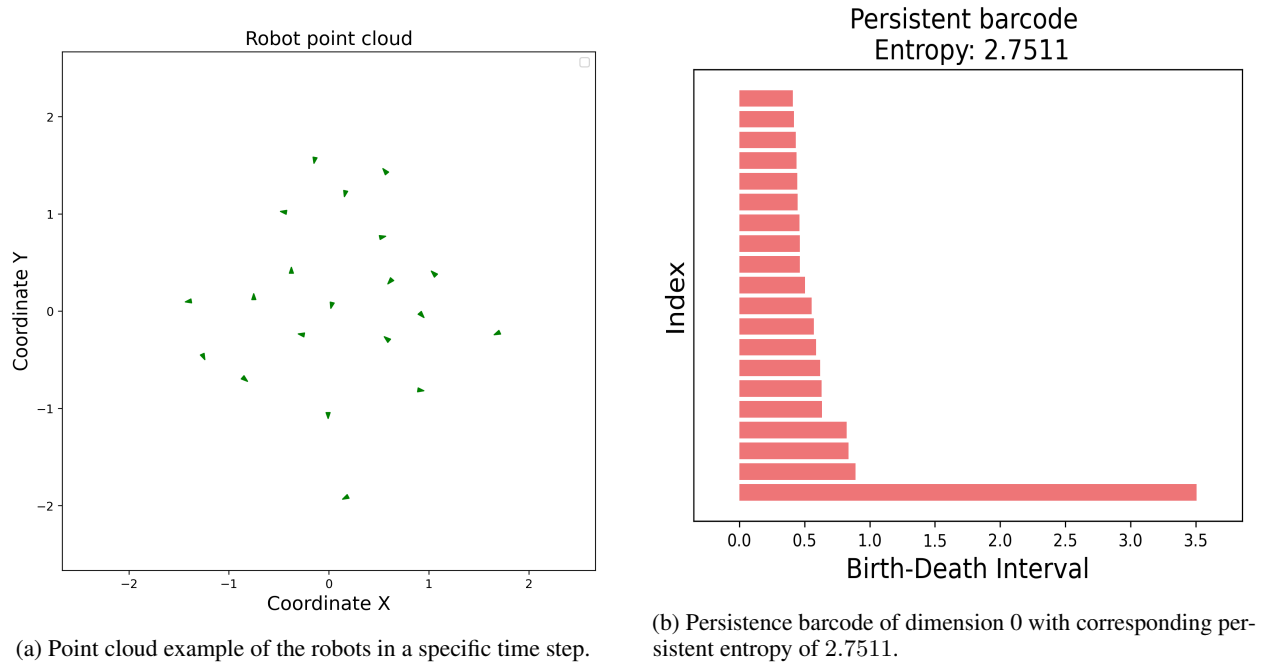


Figure 5: Illustrative example of computing the persistent entropy of a robot point cloud.

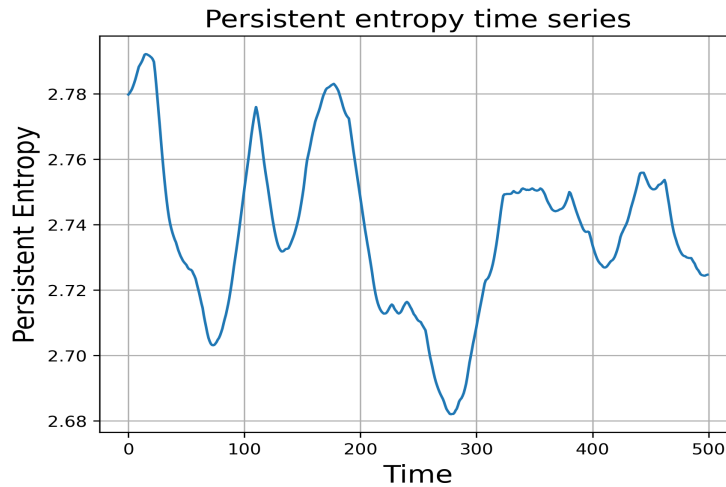


Figure 6: Persistent entropy time series example of a simulation.

are constructed using order statistics methods to the classifier, such as probabilistic scaling and conformal prediction. In addition, we extract local rules from these safety regions using Anchors.

Note that a specific time step in a simulation with a higher persistent entropy indicates a greater dispersion among the robots in relation how they are distributed around the space, without clusters of robots in certain areas and without empty areas or areas with few robots, being less likely to have empty areas and to form cluster of robots very grouped and another ones very far away, while a lower entropy indicates that less dispersion between the robots, being more likely to occupy specific regions of space and form clusters. See Fig. 7 for an illustrative example, where we can compare the robot point cloud of two different time steps, the point cloud on the left with lower entropy than the one on the right (where the points are more dispersed).

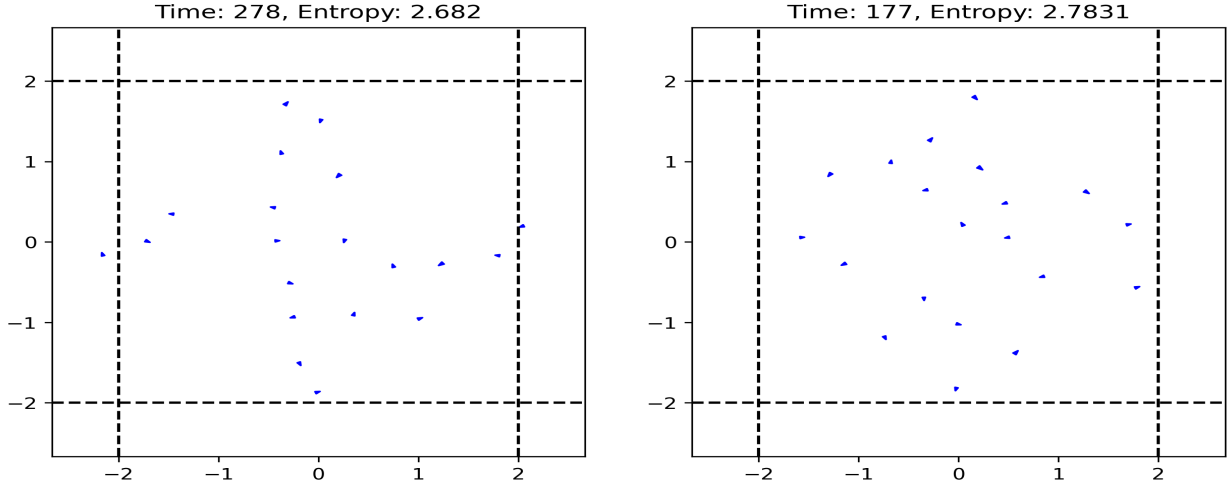


Figure 7: Point clouds of two different time steps with the corresponding persistent entropy on top.

## 5 Experiments

In this section, we present the experiments and results we carried out by putting together the simulator, the safety regions and the illustrated topological techniques. After data collection through Navground simulator, we study the problem of collision avoidance, comparing our methodology with the one that uses behavior parameters ( $\sigma$ ,  $\eta$  and  $\tau$ , which are defined in Tab. 1 for the construction of safety regions [17] (instead of the topological features), then studying the problem of deadlock avoidance, and finally combining them for safe and efficient (free of collisions and deadlocks) navigations.

### 5.1 Data Collection

Using Navground, we generated a suitable dataset to study the safety of robots' movement while avoiding collisions, deadlocks, and both of them, via probabilistic scaling and conformal prediction methods, with interpretation via rule-based classifiers. We executed  $N = 10000$  simulation runs, each with 2000 time steps, each one separated from the previous one in 0.1 seconds, with a group of 20 robots modelled after the Thymio robot. Each simulated robot executes the HL navigation with the following parameters (behavior parameters of the simulations):

- $v_{\text{opt}} = 0.12$  m/s
- $\tau_{\text{rot}} = 0.5$  s
- $\sigma$  sampled uniformly from  $[0.0 \text{ m}, 0.1 \text{ m}]$  for collision avoidance, and from  $[0.0 \text{ m}, 0.5 \text{ m}]$  for deadlock avoidance and for safe and efficient simulations (since there are hardly any simulations with deadlocks if we limit this parameter to 0.1).
- $\tau$  and  $\eta$  sampled uniformly from  $[0.0 \text{ s}, 1.0 \text{ s}]$

These HL parameters ( $\sigma$ ,  $\eta$  and  $\tau$ ) have been sampled to generate simulations of all types, including safe, aggressive, cautious, or efficient simulations. Please, see Table 1 for an explanation of the HL parameters.

For each simulation run, we apply the methodology explained previously (Section 4), recording the following values

$$\mathbf{x} = (\text{meanEntropy}, \text{medianEntropy}, \text{stdEntropy}, \text{iqrEntropy}),$$

Then, we assigned a binary label  $y$  to each simulation through the following criteria, depending on the avoidance event:

- Safe simulation (avoiding collision):

$$y = \begin{cases} +1 & \text{if number of collisions} = 0, \\ -1 & \text{if number of collisions} > 0 \end{cases}.$$

- Efficient simulation (avoiding deadlocks):

$$y = \begin{cases} +1 & \text{if number of deadlocks} = 0, \\ -1 & \text{if number of deadlocks} > 0 \end{cases}.$$

- Compliant simulation (avoiding both, collision and deadlocks):

$$y = \begin{cases} +1 & \text{if number of collisions/deadlocks} = 0, \\ -1 & \text{if number of collisions/deadlocks} > 0 \end{cases}.$$

Finally, we obtained the dataset  $T_{\text{nav}} = \{(\mathbf{x}_j, y_j) \mid j = 1, \dots, N\}$ . In Section 5.3, we present and analyze the results obtained using reliable AI techniques for this dataset.

## 5.2 Data Exploration

Before entering in the results in terms of confidence regions and explainability, a first visual inspection of how classes are distributed in the dataset is useful to understand the non-trivial nature of the problem. In Figs. 8a, 8b and 8c, the relationships among the four persistent entropy-based metrics — mean entropy, median entropy, standard deviation of entropy (stdEntropy), and interquartile range of entropy (iqrsEntropy) — are visualized for three binary classifications: collision avoidance, deadlock avoidance, and compliant simulations (collision and deadlock avoidance). Each plot displays pairwise scatterplots, overlaid with KDE (Kernel Density Estimation) curves along the diagonals to depict distributions for each class.

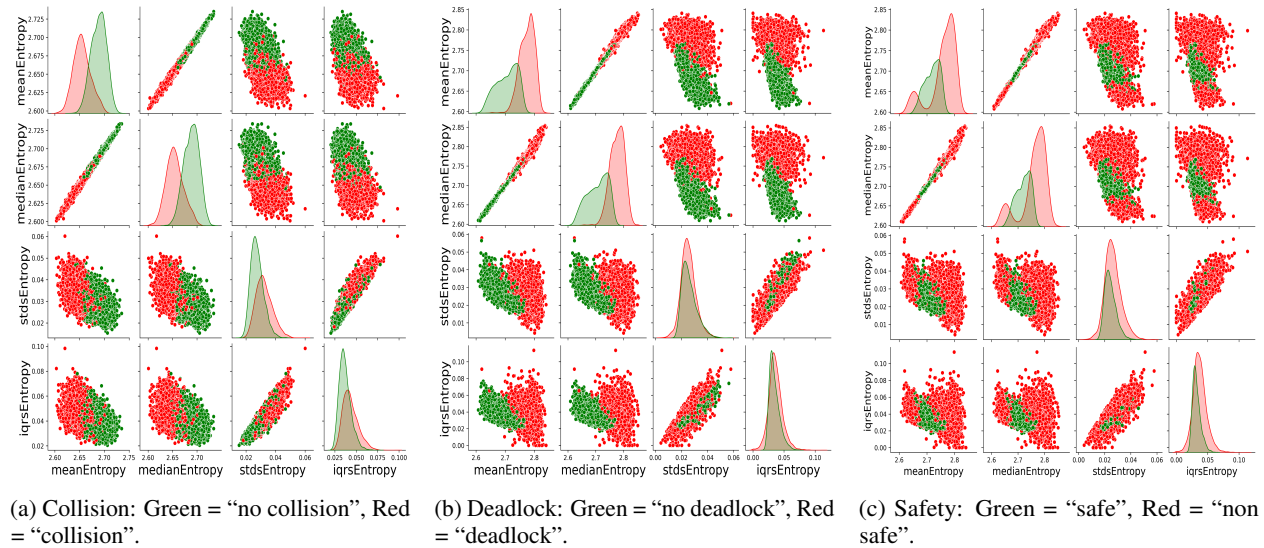


Figure 8: Pairwise class distributions of the features in  $T_{\text{nav}}$ .

Across all three classifications — collision avoidance, deadlock avoidance, and compliant simulations (collision and deadlock avoidance) — **mean entropy and median entropy** stand out as the most informative features for distinguishing between classes. While stdEntropy and iqrsEntropy provide less individual discriminatory power, they may still offer complementary information when used in combination with the other metrics. These insights highlight the potential of persistent entropy-based metrics for identifying critical system states and suggest a strong basis for further model development and optimization.

Lower values of mean entropy and median entropy are more closely associated with the “collision” class, indicating that decreased entropy in the system could signal potential collisions between robots. Higher values of mean entropy and median entropy are more closely associated with the “deadlock” class, indicating that increased entropy in the system could signal potential deadlock situations. In this way, we can observe how safe and efficient safe simulations, without collisions or deadlocks, have relatively stable values for mean entropy and median entropy, unless an extreme value occurs, either low or high.

The goal of this analysis is to characterize such a region in an interpretable way, via post-hoc rule extraction from confidence regions.

### 5.3 Results

First, we will compare training a rule-based model with the behavior parameters (as is done in [17]) against training it with the topological features extracted with this methodology for collision avoidance. For that, we will use Skope Rules. Skope Rules<sup>5</sup> is a rule-based ML algorithm, that learns interpretable and diversified rules for “scoping” a target class of interest, i.e. detecting samples from this class with high precision. In practical applications, skope-rules model has been applied to several safety-critical classification tasks, as well as anomaly detection problems or cluster description.

Table 2: Performance comparison between the adopted rule-based models. The first column reports the number of generated rules. The other columns refer to the following metrics (expressed in %): accuracy (ACC), F1-score (F1), true positive rate (TPR), false positive rate (FPR), false negative rate (FNR), true negative rate (TNR).

	# of rules	ACC	F1	TPR	FPR	FNR	TNR
SkopeRules-Behavior Parameters	8	83.6	81.9	92.0	27.5	8.0	72.5
SkopeRules-Topological Features	20	84.6	84.6	87.1	18.7	12.9	81.3

Table 2 highlights the superior performance of SkopeRules using topological features compared to behavior parameters. The topological model achieves higher accuracy (84.6% vs. 83.6%), F1-score (84.6% vs. 81.9%), and true negative rate (81.3% vs. 72.5%) while significantly reducing the false positive rate (18.7% vs. 27.5%). Although its true positive rate (87.1% vs. 92.0%) is slightly lower, and the false negative rate (12.9% vs. 8.0%) is higher, these trade-offs are outweighed by its improved balance across metrics. Remember that the positive class is the non-collision class (+1).

The use of 20 rules, compared to 8 for behavior parameters, suggests the topological model captures more complex relationships, enhancing its robustness. Models with fewer rules have the advantage of being more interpretable, but the richest ones may generate more fine-grained rules with better discriminative ability. Overall, topological features provide a more discriminative representation, making this model preferable for scenarios prioritizing accuracy and the minimization of false positives.

Also, we will compare the safety regions generated using these two types of input features. For that, the techniques detailed in Section 3.2 to derive the safety regions using Conformal Prediction and Probabilistic Scaling were applied by adopting an SVM as the classifier. Specifically, we considered a Gaussian kernel SVM, with a sigma set to 0.5, with regularization parameter set to 0.3, and a weighting of 0.5. With this base model, prior to any error control, we achieve the following performance: 78.2% accuracy, 80.6% F1 Score, 82.8% TPR, 72.7% TNR, 27.3% FPR, 17.2% FNR using behavior parameters as input and 85% accuracy, 88.1% F1 Score, 91.6% TPR, 75% TNR, 25% FPR, 8.4% FNR using topological features as input.

Table 3: Performance comparison between the adopted techniques for finding safety regions at  $\epsilon = 0.1$ . The first column refers to the input features used for training the classification models, the second refers to the adopted techniques for finding safety regions, and the third one reports the optimal scaling parameter. The other columns refer to the following metrics (expressed in %): accuracy (ACC), F1-score (F1), true positive rate (TPR), false positive rate (FPR), false negative rate (FNR), true negative rate (TNR). Probabilistic Scaling denoted as PS, and Conformal Prediction denoted as CP.

	Method	$\rho_\epsilon$	ACC	F1	TPR	FPR	FNR	TNR
Behavior parameters	PS	0.49	77.9	77	67.8	9.9	32.1	90.1
	CP	0.44	78.5	77.8	69	10.1	31	89.9
Topological Features	PS	0.42	79.8	81.6	74.3	11.9	25.7	88.1
	CP	0.21	83.7	86.2	84.1	16.9	15.9	83.1

Topological features consistently show better performance than behavior parameters across all metrics, both in baseline classification and in safety region generation. Among the methods for generating safety regions (see Table 3), Conformal Prediction demonstrates superior accuracy and F1 scores, particularly with topological features, making it the preferred approach for ensuring robust safety guarantees.

Now, we want to derive interpretable approximations for both regions in the form of decision rules. Local rule extraction via Anchors was performed on a set of instances labeled as +1 by the adjustable classifiers and sampled at a small distance  $d \leq 0.05$  from their border.

<sup>5</sup><https://github.com/scikit-learn-contrib/skope-rules>

Table 4: Performance comparison between the rules obtained using Anchors from the obtained adjustable classifiers (SVM). The first column refers to the input features used for training the adjustable classifiers, the second refers to the adopted techniques for finding safety regions, and the third column reports the number of generated rules (anchors). Covering and error percentages are reported for the logical union of the anchors being tested with respect to the labels assigned via PS ( $S_\epsilon^{PS} output$ ) and CP ( $S_\epsilon^{CP} output$ ) (Method labels column), and the real labels (Ground Truth column). Probabilistic Scaling is denoted as PS, and Conformal Prediction is denoted as CP.

	Method	# of anchors	Method labels		Ground Truth	
			Coverage	Error	Coverage	Error
Behavior Parameters	PS	5	86	36	73	29
	CP	5	85	35	73	29
Topological Features	PS	2	79	0	69	9
	CP	2	100	30	100	26

The results in Table 4 clearly demonstrate the advantages of using topological features over behavior parameters in the context of local rule extraction with Anchors. Notably, the number of generated rules (anchors) is significantly reduced when using topological features—only 2 rules ( $meanEntropy > 2.68$  and  $medianEntropy > 2.68$  for PS method, and  $meanEntropy > 2.66$  and  $medianEntropy > 2.65$  for CP method. Entropy above these values refers to simulations free of collision situations.) compared to 5 rules for behavior parameters (the same 5 rules for both methods:  $\eta > 0.75$ ,  $\tau \leq 0.5$ ,  $\tau \leq 0.25$ ,  $\tau \leq 0.76$  and  $\sigma > 0.08$ ). This reduction highlights a key advantage: the rules obtained with Topological Features are simpler, more concise, and easier to interpret, which enhances their applicability in decision-making tasks.

In addition to reducing the complexity of the rules, the performance also improves. For Topological Features, the error rates are markedly lower. For instance, under Probabilistic Scaling (PS), the Coverage Error drops to 9%, compared to 29% with behavior parameters. Even with Conformal Prediction (CP), the Coverage Error decreases to 26% while achieving a perfect 100% coverage. Despite having fewer rules, topological features maintain competitive or superior coverage compared to behavior parameters.

These findings emphasize that Topological Features not only simplify the decision rules by reducing their number but also improve their accuracy and reliability, making them a more effective and interpretable choice for defining local decision regions.

Once we have verified that the proposed methodology achieves better results for differentiating between safe (without robots collisions) and non-safe simulations, we proceed to extend its use to the case of distinguishing between efficient (without deadlocks) and non-efficient simulations. We follow exactly the same steps, but this time we do not compare the results/performance with those obtained using behavior parameters (SafetyMargin, Eta and Tau).

Using the SkopeRules method and topological features to classify simulations with deadlock cases versus efficient simulations without them, we derive a total of 18 rules, achieving highly positive performance: 89% accuracy, 88.5% F1-score, 93% TPR, and 84% TNR. This demonstrates that these features achieve even better performance for deadlock avoidance than for collision avoidance when using SkopeRules.

Next, we generate the safety regions using these features in the same manner as before. We considered a Gaussian kernel SVM, with a sigma set to 0.5, a regularization parameter set to 0.3, and a weighting of 0.5. With this base model, prior to any error control, we achieve the following performance: 86% accuracy, 82.3% F1 score, 74.7% TPR, 94.7% TNR. Using PS method we achieve the following performance:  $\rho_\epsilon$  equal to -0.12, 87.2% accuracy, 84.6% F1 score, 80.1% TPR, 92.7% TNR; and using the CP method we achieve the following performance:  $\rho_\epsilon$  equal to 0.17, 83.6% accuracy, 77.9% F1 score, 66% TPR, 97.3% TNR.

Again, local rule extraction via Anchors was performed on a set of instances labeled as +1 by the adjustable classifiers and sampled at a small distance  $d \leq 0.05$  from their border. The number of generated rules (anchors) is 2 (same for both methods:  $meanEntropy \leq 2.75$  and  $medianEntropy \leq 2.75$ . Entropy below these values refers to simulations free of deadlock situations.), so again, the rules obtained are very simpler and easier to interpret. We evaluate the logical union of the anchors being tested with respect to the labels assigned via the method used, and the real labels, obtaining the following results:

- 91% coverage and 21% error for ground truth labels, and 100% coverage and 22% for method labels for PS method.
- 91% coverage and 21% error for ground truth labels, and 100% coverage and 39% for method labels for PS method.

We can see how with the PS method we obtain a better performance in terms of error, and with the CS method a better performance in terms of covering (as for collision avoidance using topological features), although the rules are exactly the same, obviously obtaining the same performance for the real labels. Considering the non-trivial nature of the problem and of approximating a complex SVM shape via hyper-rectangular shapes (rules) while keeping the error bound as low as possible, we can consider our results as a promising compromise between safety and transparency.

Thus, if we focus on distinguishing between safe and efficient (compliant) simulations (free of collisions and deadlocks) and not compliant simulations, we obtain very simple rules for both methods:

-  $2.68 \leq \text{meanEntropy} \leq 2.75$  and  $2.68 \leq \text{medianEntropy} \leq 2.75$  for PS method.

-  $2.66 \leq \text{meanEntropy} \leq 2.75$  and  $2.65 \leq \text{medianEntropy} \leq 2.75$  for CP method.

In summary, our results highlight the advantages of using topological features in rule-based explanations and the generation of safety regions for classification. First, for differentiating between safe and non-safe simulations, we achieve better and more efficient results compared to not using these topological features. The results were even more favorable for distinguishing between efficient and non-efficient simulations, ultimately yielding a very simple rule for differentiating between compliant and non-compliant simulations. These findings confirm the suitability of topological features for enhancing transparency and reliability in classification and safety detection tasks.

## 6 Conclusions and future works

In this research, we presented an ML-based approach to compliant simulation, free of both collision and deadlock events, in mobile robot navigation. The proposed methodology contributes significantly to the field of eXplainable Artificial Intelligence (XAI) by integrating topological data analysis (TDA) and rule-based explanations to enhance interpretability in mobile robot navigation. The use of adjustable SVM classifiers and order statistics to define safety regions, followed by the extraction of Anchor rules, ensures that the decision-making process remains transparent and comprehensible. Overall, the proposed methodology achieves better and more efficient (simpler) results for collision avoidance compared to those obtained without using topological features as input in [17]. Furthermore, we extend this approach to deadlock avoidance and, ultimately, we combine the safety regions and rules for both events, obtaining the corresponding safety region and rules for safe and efficient (compliant) simulations, avoiding these two negative events (collisions and deadlocks), obtaining accurate and promising results for that. Beyond the immediate application in mobile robotics, the principles introduced in this work offer broader implications for xAI. The combination of topological insights with rule-based models presents a novel approach for generating explainable and robust decision boundaries in machine learning systems. In fields such as autonomous driving, industrial automation, and swarm robotics, where safety and efficacy are critical, the ability to construct interpretable safety regions could lead to more reliable and trustworthy AI-driven solutions.

While in this work the focus was to provide safety guarantees based on topological features, future research could explore more complex scenarios and behaviors, as well as incorporate additional topological parameters into the analysis. This could further enhance the quality of the generated safety regions, improving the interpretability, and optimizing the overall performance.

Finally, since the rules are obtained a posteriori to the simulations —meaning that we need to have the complete simulation and calculate the topological features to determine whether the simulation falls within the safety margins defined by the obtained rules—we leave as future work the definition of the simulation parameters a priori so that the resulting simulations exhibit a safe entropy value, that is, within the range identified as safe by the rules.

### Code availability

The code for the data and the experiments is available on a GitHub repository<sup>6</sup>.

### Acknowledgements

This work was partially supported by REXASI-PRO H-EU project, call HORIZON-CL4-2021-HUMAN-01-01, grant agreement ID: 101070028 and by Future Artificial Intelligence Research (FAIR) project, Italian National Recovery and Resilience Plan (PNRR), Spoke 3 - ResilientAI.

<sup>6</sup><https://github.com/Cimagroup/Topological-Features-and-Explainable-Safety-Regions>

## References

- [1] Vemuri Sudarsan Rao, Mr A Satish, and Mr BBLV Prasad. *Artificial intelligence: Principles and applications*. Leilani Katie Publication, 2024.
- [2] Demetris Vrontis, Michael Christofi, Vijay Pereira, Shlomo Tarba, Anna Makrides, and Eleni Trichina. Artificial intelligence, robotics, advanced technologies and human resource management: a systematic review. *Artificial intelligence and international HRM*, pages 172–201, 2023.
- [3] Philip Koopman and Michael Wagner. Autonomous vehicle safety: An interdisciplinary challenge. *IEEE Intelligent Transportation Systems Magazine*, 9(1):90–96, 2017.
- [4] Luca Longo, Mario Brcic, Federico Cabitza, Jaesik Choi, Roberto Confalonieri, Javier Del Ser, Riccardo Guidotti, Yoichi Hayashi, Francisco Herrera, Andreas Holzinger, et al. Explainable artificial intelligence (xai) 2.0: A manifesto of open challenges and interdisciplinary research directions. *Information Fusion*, 106:102301, 2024.
- [5] Emilio Garcia-Fidalgo and Alberto Ortiz. Vision-based topological mapping and localization methods: A survey. *Robotics and Autonomous Systems*, 64:1–20, 2015.
- [6] Naveed Islam, Khalid Haseeb, Ahmad Almogren, Ikram Ud Din, Mohsen Guizani, and Ayman Altameem. A framework for topological based map building: A solution to autonomous robot navigation in smart cities. *Future Generation Computer Systems*, 111:644–653, 2020.
- [7] Matteo Rucco, Rocio Gonzalez-Diaz, Maria-Jose Jimenez, Nieves Atienza, Cristina Cristalli, Enrico Concettoni, Andrea Ferrante, and Emanuela Merelli. A new topological entropy-based approach for measuring similarities among piecewise linear functions. *Signal Processing*, 134:130–138, 2017.
- [8] Robin R Murphy. *Introduction to AI robotics*. MIT press, 2019.
- [9] Harry A. Pierson and Michael S. Gashler. Deep learning in robotics: a review of recent research. *Advanced Robotics*, 31:821 – 835, 2017.
- [10] R Mouha. Deep learning for robotics. *Journal of Data Analysis and Information Processing*, 9:63 – 76, 2021.
- [11] Rudresh Dwivedi, Devam Dave, Het Naik, Smiti Singhal, Rana Omer, Pankesh Patel, Bin Qian, Zhenyu Wen, Tejal Shah, Graham Morgan, et al. Explainable ai (xai): Core ideas, techniques, and solutions. *ACM Computing Surveys*, 55(9):1–33, 2023.
- [12] Waddah Saeed and Christian Omlin. Explainable ai (xai): A systematic meta-survey of current challenges and future opportunities. *Knowledge-Based Systems*, 263:110273, 2023.
- [13] Davinder Kaur, Suleyman Uslu, Kaley J Rittichier, and Arjan Durresi. Trustworthy artificial intelligence: a review. *ACM computing surveys (CSUR)*, 55(2):1–38, 2022.
- [14] Sule Anjomshoae, Amro Najjar, Davide Calvaresi, and Kary Främling. Explainable agents and robots: Results from a systematic literature review. In *18th International Conference on Autonomous Agents and Multiagent Systems (AAMAS 2019), Montreal, Canada, May 13–17, 2019*, pages 1078–1088. International Foundation for Autonomous Agents and Multiagent Systems, 2019.
- [15] Shahin Atakishiyev, Mohammad Salameh, Hengshuai Yao, and Randy Goebel. Explainable artificial intelligence for autonomous driving: A comprehensive overview and field guide for future research directions. *IEEE Access*, 2024.
- [16] Alberto Carlevaro, Teodoro Alamo, Fabrizio Dabbene, and Maurizio Mongelli. Probabilistic safety regions via finite families of scalable classifiers. *arXiv preprint arXiv:2309.04627*, 2023.
- [17] Sara Narteni, Alberto Carlevaro, Jérôme Guzzi, and Maurizio Mongelli. Ensuring safe social navigation via explainable probabilistic and conformal safety regions. In Luca Longo, Sebastian Lapuschkin, and Christin Seifert, editors, *Explainable Artificial Intelligence*, pages 396–417, Cham, 2024. Springer Nature Switzerland.
- [18] Allen Hatcher. *Algebraic topology*. Cambridge University Press, 2005.
- [19] Gunnar Carlsson. Topological methods for data modelling. *Nature Reviews Physics*, 2(12):697–708, 2020.
- [20] Herbert Edelsbrunner and John L Harer. *Computational topology: an introduction*. American Mathematical Society, 2022.
- [21] F. de la Paz López and J. R. Álvarez Sánchez. Topological maps for robot’s navigation: A conceptual approach. In José Mira and Alberto Prieto, editors, *Bio-Inspired Applications of Connectionism*, pages 459–467, Berlin, Heidelberg, 2001. Springer Berlin Heidelberg.
- [22] Miriam Esteve and Antonio Falcó. tramotda: A trajectory monitoring system using topological data analysis. *SoftwareX*, 28:101953, 2024.



- [23] Jumman Hossain, Abu Zaher Md Faridee, Nirmalya Roy, Jade Freeman, Timothy Gregory, and Theron Trout. Toponav: Topological navigation for efficient exploration in sparse reward environments. pages 693–700, 10 2024.
- [24] Harish Chintakunta, Thanos Gentimis, Rocio Gonzalez-Diaz, Maria-Jose Jimenez, and Hamid Krim. An entropy-based persistence barcode. *Pattern Recognition*, 48(2):391–401, 2015.
- [25] Matteo Rucco, Filippo Castiglione, Emanuela Merelli, and Marco Pettini. Characterisation of the idiotypic immune network through persistent entropy. In *Proceedings of ECCS 2014: European conference on complex systems*, pages 117–128. Springer, 2016.
- [26] Nieves Atienza, Rocio Gonzalez-Diaz, and Matteo Rucco. Persistent entropy for separating topological features from noise in vietoris-rips complexes. *Journal of Intelligent Information Systems*, 52:637–655, 2019.
- [27] Pek Y Lum, Gurjeet Singh, Alan Lehman, Tigran Ishkanov, Mikael Vejdemo-Johansson, Muthu Alagappan, John Carlsson, and Gunnar Carlsson. Extracting insights from the shape of complex data using topology. *Scientific reports*, 3(1):1236, 2013.
- [28] Vikas Hassija, Vinay Chamola, Atmesh Mahapatra, Abhinandan Singal, Divyansh Goel, Kaizhu Huang, Simone Scardapane, Indro Spinelli, Mufti Mahmud, and Amir Hussain. Interpreting black-box models: a review on explainable artificial intelligence. *Cognitive Computation*, 16(1):45–74, 2024.
- [29] Jakob Jonsson. *Simplicial complexes of graphs*, volume 1928. Springer, 2008.
- [30] James R Munkres. *Elements of algebraic topology*. CRC press, 2018.
- [31] Robert Ghrist. Barcodes: the persistent topology of data. *Bulletin of the American Mathematical Society*, 45(1):61–75, 2008.
- [32] Vladimir Vovk. Cross-conformal predictors. *Annals of Mathematics and Artificial Intelligence*, 74:9–28, 2015.
- [33] Alberto Carlevaro, Teodoro Alamo, Fabrizio Dabbene, and Maurizio Mongelli. Conformal predictions for probabilistically robust scalable machine learning classification. *Machine Learning*, 113(9):6645–6661, 2024.
- [34] Christoph Molnar. *Interpretable Machine Learning*. 2 edition, 2022.
- [35] Lucas Rizzo, Damiano Verda, Serena Berretta, and Luca Longo. A novel integration of data-driven rule generation and computational argumentation for enhanced explainable ai. *Machine Learning and Knowledge Extraction*, 6(3):2049–2073, 2024.
- [36] Jérôme Guzzi, Alessandro Giusti, Luca M. Gambardella, Guy Theraulaz, and Gianni A. Di Caro. Human-friendly robot navigation in dynamic environments. In *2013 IEEE International Conference on Robotics and Automation*, pages 423–430, 2013.